

AD \_\_\_\_\_

CONTRACT NUMBER: DAMD17-94-C-4047

TITLE: Crystallographic Studies of the Anthrax Lethal Toxin

PRINCIPAL INVESTIGATOR: Christin A. Frederick, Ph.D.

CONTRACTING ORGANIZATION: Dana Farber Cancer Institute  
Boston, Massachusetts 02115-6084

REPORT DATE: July 1996

TYPE OF REPORT: Annual

PREPARED FOR: Commander  
U.S. Army Medical Research and Materiel Command  
Fort Detrick, Frederick, Maryland 21702-5012

DISTRIBUTION STATEMENT: Approved for public release;  
distribution unlimited

The views, opinions and/or findings contained in this report are those of the author(s) and should not be construed as an official Department of the Army position, policy or decision unless so designated by other documentation.

19960917 079

DTIC QUALITY INSPECTED 1

# REPORT DOCUMENTATION PAGE

*Form Approved*  
**OMB No. 0704-0188**

Public reporting burden for this collection of information is estimated to average 1 hour per response, including the time for reviewing instructions, searching existing data sources, gathering and maintaining the data needed, and completing and reviewing the collection of information. Send comments regarding this burden estimate or any other aspect of this collection of information, including suggestions for reducing this burden, to Washington Headquarters Services, Directorate for Information Operations and Reports, 1215 Jefferson Davis Highway, Suite 1204, Arlington, VA 22202-4302, and to the Office of Management and Budget, Paperwork Reduction Project (0704-0188), Washington, DC 20503.

<b>1. AGENCY USE ONLY (Leave blank)</b>		<b>2. REPORT DATE</b> July 1996	<b>3. REPORT TYPE AND DATES COVERED</b> Annual (1 Jul 95 - 30 Jun 96)	
<b>4. TITLE AND SUBTITLE</b> Crystallographic Studies of the Anthrax Lethal Toxin			<b>5. FUNDING NUMBERS</b> DAMD17-94-C-4047	
<b>6. AUTHOR(S)</b> Christin A. Frederick, Ph.D.				
<b>7. PERFORMING ORGANIZATION NAME(S) AND ADDRESS(ES)</b> Dana Farber Cancer Institute Boston, Massachusetts 02115-6084			<b>8. PERFORMING ORGANIZATION REPORT NUMBER</b>	
<b>9. SPONSORING/MONITORING AGENCY NAME(S) AND ADDRESS(ES)</b> Commander U.S. Army Medical Research and Materiel Command Fort Detrick, Frederick, Maryland 21702-5012			<b>10. SPONSORING/MONITORING AGENCY REPORT NUMBER</b>	
<b>11. SUPPLEMENTARY NOTES</b>				
<b>12a. DISTRIBUTION / AVAILABILITY STATEMENT</b> Approved for public release; distribution unlimited			<b>12b. DISTRIBUTION CODE</b>	
<b>13. ABSTRACT (Maximum 200)</b>  The lethal form of Anthrax results from the inhalation of anthrax spores. Death is primarily due to the effects of the lethal toxin (Protective Antigen (PA) + Lethal Factor) from the causative agent, <i>Bacillus anthracis</i> . All the Anthrax vaccines currently in use or under development contain or produce PA, the major antigenic component of anthrax toxin, and there is a clear need for an improved vaccine for human use. In the previous report we described the first atomic resolution structure of PA, revealing that the molecule is composed largely of $\beta$ -sheets organized into four domains. This information can be used in the design of recombinant PA vaccines. In this report we describe additional features of the full-length PA molecule derived from further crystallographic refinement and careful examination of the structure. We compare two crystal forms of PA grown at different pH values and discuss the functional implications. A complete definition of the function of each domain must await the crystal structure of the PA <sub>63</sub> heptamer. We have grown crystals of the heptamer under both detergent and detergent-free conditions, and made substantial progress towards the crystal structure. The mechanism of anthrax intoxication in the light of our results is reviewed.				
<b>14. SUBJECT TERMS</b>  Anthrax, Protective Antigen, Vaccine			<b>15. NUMBER OF PAGES</b> 30	
			<b>16. PRICE CODE</b>	
<b>17. SECURITY CLASSIFICATION OF REPORT</b> Unclassified	<b>18. SECURITY CLASSIFICATION OF THIS PAGE</b> Unclassified	<b>19. SECURITY CLASSIFICATION OF ABSTRACT</b> Unclassified	<b>20. LIMITATION OF ABSTRACT</b> Unlimited	

FOREWORD

Opinions, interpretations, conclusions and recommendations are those of the author and are not necessarily endorsed by the US Army.

N/A  Where copyrighted material is quoted, permission has been obtained to use such material.

N/A  Where material from documents designated for limited distribution is quoted, permission has been obtained to use the material.

NA  Citations of commercial organizations and trade names in this report do not constitute an official Department of Army endorsement or approval of the products or services of these organizations.

NA  In conducting research using animals, the investigator(s) adhered to the "Guide for the Care and Use of Laboratory Animals," prepared by the Committee on Care and Use of Laboratory Animals of the Institute of Laboratory Resources, National Research Council (NIH Publication No. 86-23, Revised 1985).

NA  For the protection of human subjects, the investigator(s) adhered to policies of applicable Federal Law 45 CFR 46.

In conducting research utilizing recombinant DNA technology, the investigator(s) adhered to current guidelines promulgated by the National Institutes of Health.

In the conduct of research utilizing recombinant DNA, the investigator(s) adhered to the NIH Guidelines for Research Involving Recombinant DNA Molecules.

NA  In the conduct of research involving hazardous organisms, the investigator(s) adhered to the CDC-NIH Guide for Biosafety in Microbiological and Biomedical Laboratories.

  
PI - Signature 7/17/96  
Date

## TABLE OF CONTENTS

### INTRODUCTION

1. Background 2
2. Purpose and scope of research 3
3. Previous work 3
4. Outline of current report 3

### BODY

1. Refinement of the Protective Antigen model 4
2. Description of the PA Structure 4
  - a. Domain 1 5
  - b. Domain 2 6
  - c. Domain 3 6
  - d. Domain 4 6
3. Two crystal forms of PA compared 7
4. Homology with Iota-Ib and VIP1 8
5. Crystallographic studies of the PA<sub>63</sub> heptamer 8
6. Insights into PA activity 10
  - a. Receptor binding 10
  - b. EF/LF binding 10
  - c. Heptamer formation 11
  - d. Membrane insertion 11

### CONCLUSIONS 12

### FIGURES

1. Steps in anthrax intoxication of the host cell 14
2. Ribbon diagram of PA 15
3. Domain 1 16
4. The calcium binding site 17
5. Domain 2 18
6. Domain 3 19
7. Domain 4 20
8. Secondary structure and sequence alignment 21
9. Hypothetical model of the PA<sub>63</sub> heptamer 22
10. A possible mechanism of membrane insertion 23

### REFERENCES 24

### BIBLIOGRAPHY 27

## **INTRODUCTION**

### **1. Background**

The study of anthrax has played an important role in the history of medicine, leading to the establishment of Koch's postulates (1) and to the development of the first bacterial vaccine (2, 3). Outbreaks of anthrax continue to be reported, particularly in developing nations (4). Public awareness has been greatly raised by recent investigations into the Sverdlovsk outbreak of 1979 (5-7) and by the threat of anthrax spores being used as an agent of biological warfare (8).

Anthrax is caused by the spore-forming bacterium, *Bacillus anthracis*, and primarily afflicts herbivores such as cattle and sheep (9). Humans acquire the disease from infected animals or their products in one of three forms: a cutaneous form characterized by black pustules; a gastrointestinal form caused by eating contaminated meat; and a pulmonary form caused by inhaling anthrax spores, which is usually fatal within a few days of infection (10).

Two factors account for the virulence of *B. anthracis*: a poly-D-glutamic acid capsule that protects against bactericidal components of host sera (11), and "anthrax toxin". Anthrax toxin refers collectively to three secreted proteins: the edema factor (EF, 89 kDa), the lethal factor (LF, 90 kDa), and the protective antigen (PA, 83 kDa) (12). Although these proteins are individually non-toxic, PA combined with EF produces edema in the skin of guinea pigs and rabbits (13), while PA combined with LF lyses mouse macrophages (14) and induces death in experimental animals (15).

The action of anthrax toxin on the host cell has recently been reviewed (12), and is illustrated in figure 1. PA binds with high affinity ( $K_d \sim 1$  nM) to a protein receptor found on most mammalian cells (11, 16). Cleavage by a cell-surface protease, probably furin (17, 18), releases an N-terminal 20 kDa fragment, PA<sub>20</sub>, and permits the 63 kDa fragment, PA<sub>63</sub>, to form a heptamer (19) and to bind LF or EF with high affinity ( $K_d = 10$  pM) (11). The complex of PA<sub>63</sub> with LF or EF then undergoes receptor-mediated endocytosis (20). Acidification of the endocytic vesicle leads to insertion of PA<sub>63</sub> into the endosomal membrane and translocation of EF or LF into the cytosol, where they exert toxic catalytic effects: calmodulin-dependent adenylate cyclase activity in the case of EF (21, 22); and an unknown activity in the case of LF. In the "A-B" toxin nomenclature (23) PA is the B (binding) moiety, and LF and EF are alternative A (enzymatically active) moieties.

PA is the most immunogenic of the three anthrax toxin proteins (24, 25) and, as implied by its name, is the principal active component in anthrax vaccines (26). In the United States, the currently licensed human vaccine, MDPH-PA, is obtained from a non-virulent strain of *B. anthracis* and consists of aluminum hydroxide-adsorbed supernatant

material, which is primarily PA (27). Immunization with MDPH-PA requires multiple doses, produces undesired side-effects in some individuals, and has diminished efficacy against certain virulent strains of *B. anthracis* (27-29). There is therefore an obvious need to improve the efficacy of the human vaccine.

## **2. Purpose and scope of research**

The work described here aims at determining the atomic resolution structure of the anthrax protective antigen in its monomeric and oligomeric forms. These structures should lead to a greater understanding of anthrax intoxication by providing insight into the receptor binding, EF/LF binding, oligomerization, membrane channel formation, and EF/LF translocation activities of PA. This information should aid in the development of an improved vaccine by facilitating the construction of recombinant proteins that are deficient in key activities but retain high immunogenicity. It should also benefit new biomedical applications, such as the use of anthrax toxin as a "targeted toxin" (30).

## **3. Previous work**

At this time last year we had solved the crystal structure of PA using two crystal forms and had partially refined the atomic model, which had a crystallographic R factor of 29% at 2.1 Å resolution. We showed that the molecule was largely composed of  $\beta$  strands and was organized into four domains. We used the results of previously reported biochemical and mutagenesis experiments to assign each domain a putative function. In addition, we had grown crystals of the PA<sub>63</sub> heptamer and set out to determine its crystal structure. Based on available electron microscopy data, we were able to build a hypothetical model of the heptamer.

## **4. Outline of current report**

In this report we describe additional features of the full-length PA molecule discovered as a result of further crystallographic refinement and careful examination of the structure. We discuss the differences observed between the two PA crystal forms used in the structure determination. We also report the progress made in solving the crystal structure of the PA<sub>63</sub> heptamer. Finally, we review the mechanism of anthrax intoxication in the light of our results.

## BODY

### 1. Refinement of the Protective Antigen model

Two crystal forms were used in the structure determination. Crystal form 1, grown at pH 7.5, diffracted synchrotron radiation to 2.5 Å spacing, while crystal form 2, grown at pH 6.0, diffracted to 2.1 Å. The current refinement statistics for the two crystal forms are listed in table 1. The model for crystal form 1 contains 680 (out of 735) residues, 2 calcium ions and no water molecules, and will be further refined. The model for crystal form 2 consists of 660 residues, 310 water molecules and 2 calcium ions, and its refinement is essentially complete. No density is seen in either crystal form for residues 1-13, 162-176 and 304-319, consistent with the protease sensitivity of these regions (11). Several differences exist between the two crystal forms, as described below. 88% of the backbone angles are in the most favored regions of the Ramachandran plot, with none in disallowed regions. The electron density in most regions of the  $2F_o - F_c$  map is of excellent quality.

Crystal Form	Space Group and Cell Dimensions	Resolution (Å)	R factor (%)	R (free) (%)	rms bond lengths (Å)	rms bond angles
1 (pH 7.5)	P2 <sub>1</sub> 2 <sub>1</sub> 2 <sub>1</sub> a=119.8 b=73.8 c=95.0	6-2.5	27.1	32.0	0.009	2.0°
2 (pH 6.0)	P2 <sub>1</sub> 2 <sub>1</sub> 2 <sub>1</sub> a= 99.3 b=93.7 c=82.0	6-2.1	22.9	28.1	0.006	1.5°

**Table 1.** Refinement statistics of the two crystal forms of PA. Form-1 crystals grow by the hanging drop method from 14-18% PEG 1000, 10% glycerol and 50 mM HEPES pH 7.5 at 4° C. Form-2 crystals grow from 12-18% PEG 8K and 50 mM citrate pH 6.0 at 4°C.

### 2. Description of the PA Structure.

A ribbon diagram of PA is shown in figure 2. The molecule has approximate dimensions 100 Å x 70 Å x 40 Å, and is organized into four domains. These are composed primarily of antiparallel β sheets with only a few short α helices. Domains 1 and 2 are roughly equal in size and twice as large as domains 3 and 4. The cleavage by furin which results in the PA<sub>20</sub> and PA<sub>63</sub> fragments does not occur between domains, but within domain 1. The domain assignments are summarized in table 2.

(Sub)domain	Residues	Activity	Furin fragment
1a	1-167	blocks oligomerization and EF/LF binding	PA <sub>20</sub>
1b	168-258	Ca <sup>2+</sup> binding	
2	259-487	EF/LF binding * oligomerization * membrane insertion *	PA <sub>63</sub>
3	488-595	EF/LF binding *	
4	596-735	receptor binding	

**Table 2.** Domains of PA. 1a and 1b are subdomains of domain 1 defined by the furin cleavage site. Residues 1-167 are referred to as subdomain 1a when part of the full-length PA molecule, and as PA<sub>20</sub> after dissociating as a proteolytic fragment. Putative activities are indicated by an asterisk.

**a. Domain 1.** Domain 1 contains a large  $\beta$  sheet made of nine strands and a smaller sheet of five strands (Fig. 3). The furin cleavage site at the sequence RKKR<sup>167</sup> is located in an exposed loop for which no density is seen. The cleavage site divides domain 1 into two subdomains, referred to as 1a and 1b (table 2). Subdomain 1a, which forms the PA<sub>20</sub> fragment, is a  $\beta$ -sandwich with jelly roll topology, and comprises the small sheet plus six strands of the large sheet. Subdomain 1b contains the remaining strands of the large sheet and three short helices. Thus, the large sheet spans the cleavage site and becomes torn between strands 2 and 13 when PA<sub>20</sub> dissociates from PA<sub>63</sub>. The interface between the two subdomains buries 2600 Å<sup>2</sup> of accessible surface area, and involves several hydrophobic residues of subdomain 1b. The extensive interface explains why PA can be “nicked” in vitro without dissociating into two fragments (11). Subdomain 1b is probably involved in EF/LF binding (see below).

In the course of refining the structure of PA we discovered two strong peaks of density in an F<sub>0</sub>-F<sub>c</sub> difference map that were located in subdomain 1b. These peaks were identified as calcium ions on the basis of coordination geometry, bond distances, and the prevalence of acidic ligands. This finding was confirmed by atomic absorption

spectroscopy measurements: PA was found to bind calcium with a PA:Ca stoichiometry of 1:1.4; no other metals tested bound to any significant extent (T. Koehler and R.J.Collier, unpublished). The calcium binding site is illustrated in figure 4. The two calcium ions are 4.3 Å apart, and octahedral coordination is provided by residues 177-188 and 222-235. Residues 177-188 form a calcium-binding loop similar to that found in the canonical EF hand (31). Residues 222-235 do not resemble a known calcium binding motif. Of the twelve calcium ligands, eight are carboxylate oxygens of acidic residues, three are main chain carbonyl oxygens and one is a water molecule (Fig. 4). Three acidic residues bind both ions. The ions are buried within subdomain 1*b* and play a clear role in stabilizing its three-dimensional structure.

**b. Domain 2.** Domain 2 is the longest domain (~65 Å) and is dominated by a β barrel (Fig. 5). The front and back faces of the barrel are quite flat and give domain 2 a wedge-like shape. At the wide edge of this wedge the barrel contains a deep cleft (Fig. 5). The domain also contains four prominent loops: loop 1 is composed entirely of hydrophilic residues, and is mostly disordered. Loop 2, also disordered, contains two Phe residues (F313 and F314) at its tip and is susceptible to proteolysis by chymotrypsin (11). Loop 3 is ordered in crystal form 1 (grown at pH 7.5) and contains three buried hydrophobic residues, but is disordered in crystal form 2 (grown at pH 6.0). Our studies indicate that the difference in conformation is due to the pH difference (see below). Loop 4 contains an exposed phenylalanine, F427, which is in a crystal contact (in both crystal forms) with domain 3 of another molecule. We suggest that domain 2 mediates heptamer formation and membrane insertion, with loops 2 to 4 playing important roles (see below).

**c. Domain 3.** Domain 3 is the smallest of the domains and contains a four-stranded β sheet, a hairpin, and four helices (Fig.6). One of the helices protrudes significantly from the body of the molecule (Fig. 6, top). This helix is part of a stretch of residues (511-517) that are ordered in crystal form 1 but form a disordered loop in crystal form 2. The longest helix in domain 3 is part of a triangular strand-helix-loop structure that permits five hydrophobic residues to form a flat, solvent-exposed, hydrophobic "patch" (Fig. 6). In crystals of PA this patch is occupied by residue F427 from domain 2 of another molecule, as mentioned above. Domain 3 likely interacts with EF and LF (see below).

**d. Domain 4.** Domain 4 contains a sandwich of two 4-stranded antiparallel β sheets, and a β-hairpin that packs intimately against domain 3 (Fig. 7). There is also a large loop (residues 703-720) which forms part of the interface between domains 2 and

4. Considerable evidence, listed below, indicates that domain 4 is the receptor binding domain.

### 3. Two crystal forms of PA compared

The models of PA corresponding to the two crystal forms were compared by superimposing the main chain atoms by a least-squares fit procedure. The overall rms deviation for the backbone atoms is 1.15 Å (table 3*a*). Superimposing the individual domains showed that the shifts were smallest in domain 3 and greatest in domain 1 (table 3*a*). Apart from two loops (residues 274-286 and 422-432) involved in crystal contacts in form 1 but not in form 2, there are three other regions that are ordered in one crystal form and disordered in the other. These are listed in table 3*b*. Residues 208-212 form a disordered loop in crystal form 1 but in crystal form 2 they form a small helix which buries His211. Conversely, residues 340-352 and 511-516 are ordered in crystal form 1 and disordered in form 2.

<b>a</b>	<b>Domain</b>	<b>RMS Shift (Å)</b>	
	1	1.29	
	2	0.72	
	3	0.54	
	4	0.75	
	Overall	1.15	

<b>b</b>	<b>Form 1</b>		<b>Form 2</b>
<b>Residues</b>	<b>pH 7.5</b>	<b>pH 6.0<sup>†</sup></b>	<b>pH 6.0</b>
208-12	disordered	disordered	helix
340-52	helix	disordered	disordered
511-16	helix	helix	disordered

**Table 3.** Comparison of the PA models for the two crystal forms. *a*) Models for the two crystal forms of individual domains or of the entire molecule were superimposed by a least-squares fit and the overall RMS deviation determined for main-chain atoms. *b*) Residues listed are ordered in one crystal form and disordered in the other.

<sup>†</sup>3.0 Å data set obtained from a form-1 crystal soaked in harvest buffer at pH 6.0.

These conformational differences may be due to different crystal lattices or to the different pH conditions used to grow the crystals (pH 7.5 for form 1 and pH 6.0

for form 2). To determine the cause of these changes, a 3.0 Å data set was collected from form-1 crystals soaked in harvesting buffer at pH 6. The model of crystal form 1 (minus the 3 stretches listed in table 3b) was refined and  $2F_o-F_c$  and  $F_o-F_c$  omit maps were calculated. The conformations of residues 511-16 and 208-212 were found to be the same as at pH 7.5, but residues 340-352 were disordered, suggesting that their conformation had been influenced by the change in pH. These residues comprise loop 3 in domain 2 and contain three hydrophobic residues, Trp346, Met350 and Leu352, that are buried inside the core of the barrel of domain 2 in crystal form 1 (figure 5). Their exposure at pH 6.0 might be related to the ability of PA<sub>63</sub> to insert into membranes at acidic pH.

#### 4. Homology with Iota-Ib and VIP1.

In last year's report we remarked on the sequence homology between PA and the iota-Ib toxin of *Clostridium perfringens*, and used this information to support our putative assignment of domain function. We have recently obtained the sequence of another bacterial toxin homologous to PA, the vegetative insecticidal protein, VIP1, of *Bacillus cereus* (Greg Warren, personal communication), allowing us to extend our previous analysis. Like the anthrax and iota toxins, the VIP toxin is binary, i.e., the "A" (VIP2) and "B" (VIP1) parts exist as separate polypeptides. Like PA and Iota-Ib, VIP1 is produced in a proform that binds to host cell receptors and becomes proteolytically activated at a site corresponding to the furin cleavage site of PA.

PA shares 32% sequence identity with iota-Ib and 27% with VIP1. The sequence alignment is shown in figure 8. 19% of the sequence is identical in all three proteins, with (sub)domains 1a, 1b, 2, 3 and 4 displaying 13, 26, 25, 21 and 10 % sequence identity, respectively. The low degree of identity in subdomain 1a is not surprising given that it plays no further role in intoxication after being removed (as PA<sub>20</sub>) on the cell surface. Except in domain 4, strands and helices are mostly conserved (Fig. 8), suggesting that VIP1 and iota-Ib have the same domain organization as PA, with similar folds for domains 1 to 3. Residues in PA involved in calcium binding are identical in VIP1 and iota-Ib, except for two residues (S222 and K225) which bind through a backbone carbonyl (Fig. 4); thus, VIP1 and iota-Ib likely also bind calcium. Of the 144 residues identical among the three proteins, ~65 are buried in the molecule's hydrophobic core. Many of the remaining residues cluster on the two faces of domain 2 (data not shown), and may form part of a conserved interface within the PA<sub>63</sub> heptamer (see below).

#### 5. Crystallographic studies of the PA<sub>63</sub> heptamer

In last year's annual report we noted that we had grown small crystals of the PA<sub>63</sub> heptamer and collected low-resolution diffraction data. We experienced

difficulties reproducing results because of the instability of PA<sub>63</sub>. In particular, the protein loses its ability to form ordered crystals after a few days of being stored at 4 °C. Furthermore, crystals have a short shelf-life of only ~3 days, after which they start to develop cracks and cease to diffract. We have overcome this problem by freezing aliquots of PA<sub>63</sub> at -80 °C immediately following purification, and by only using crystals that are freshly grown from recently thawed protein in our diffraction experiments.

Using this procedure we reproduced the original crystal form of PA<sub>63</sub> and grew two additional crystal forms. These are summarized in table 4. The original crystal form, form 1, is the best characterized of the three. These crystals have a high solvent content, and are very fragile. To collect a complete data set from a single crystal it is necessary to flash-freeze the crystal in liquid nitrogen to prevent radiation damage. By this method we were able to collect a complete data set for crystal form 1 at 8.0 Å resolution using PEG 200 as the cryoprotectant. A self-rotation function revealed that the 7-fold axis of the heptamer is parallel to the two-fold screw axis. We used these results and a model derived from the PA crystal structure to carry out an exhaustive crystal packing analysis to determine what were the possible orientations available for monomers to adopt within the heptamer. The packing analysis indicated that less than 30% of orientation space was available to monomers, and we used this information to refine the hypothetical model of the heptamer that we had previously built (see below).

Crystal Form	Crystallization conditions	Space Group	Cell Dimensions	Diffraction Limit (Å)	No. heptamers possible/ asym. unit	% Solvent Content
1	1-5% PEG 8000, 80-150 mM CaCl <sub>2</sub> , 50 mM TRIS pH 8.5-9.0	P2 <sub>1</sub>	a=131 b=148 c=157 β=105°	5.5	1	64
2	Same as above	P2 <sub>1</sub> or P2	a=184 b=208 c=227 β=110°	5.2	1 2 3 4	87 74 61 48
3	200 mM Li <sub>2</sub> SO <sub>4</sub> , 50-70 mM β-octylglucoside, 50 mM TRIS pH 8.5	C2	a=174 b=205 c=131 β=95°	at least 7	1	55

**Table 4.** Crystal forms of the PA<sub>63</sub> heptamer.

The 8 Å data set that we collected from crystal form 1 did not allow us to solve the structure by molecular replacement because of the lack of high resolution data. Recently, using synchrotron radiation we found that crystals mounted at room

temperature in capillaries diffract well to 5.5Å, with some spots visible at 4.9Å. Only 2-3 degrees of data can be collected from each crystal before it decays due to radiation damage, but by using a large number of crystals it should be possible to collect a complete data set. At this resolution we expect to be able to obtain a unique solution by molecular replacement. We have also been searching for heavy metal derivatives in an attempt to obtain experimental phases by multiple isomorphous replacement (MIR). Because the crystals are so fragile, soaking them in heavy metal compounds leads to disruption of the crystal lattice. However, we have succeeded in co-crystallizing PA<sub>63</sub> in the presence of platinum chloride and methylmercuric nitrate, compounds which provided useful heavy metal derivatives in solving the structure of full-length PA. It is anticipated that these compounds will also derivatize the PA<sub>63</sub> heptamer. The phases obtained either by molecular replacement or MIR can be greatly improved by exploiting the seven-fold non-crystallographic symmetry of the crystal, and these improved phases should provide us with electron density maps of very high quality.

Crystal form 2 grows under the same conditions and displays the same morphology as crystal form 1. However, form-2 crystals have a larger unit cell (table 4) and are more stable to X-rays than form-1 crystal. Form-2 crystals diffract well to about 5.2 Å spacing, with some spots visible at 4.7 Å resolution. The cell dimensions suggest that up to four heptamers can be accommodated per asymmetric unit.

Crystal form 3 grows in the presence of the detergent β-octylglucoside and displays a different morphology to the other two crystal forms. The requirement for detergent may reflect a different conformation of the molecule than is present in the other two crystal forms. On our home source these crystals diffract to 7 Å spacing, and we anticipate a higher diffraction limit using synchrotron radiation.

## 6. Insights into PA activity.

**a. Receptor binding.** There is considerable evidence that the binding of PA to cells is mediated by domain 4. A chymotryptic fragment made of residues 314-735 can bind to cells whereas residues 1-313 cannot (32); antibodies that recognize an epitope between residues 671 to 721 block the binding of PA to the cell surface (33); and the deletion of 3, 5 or 7 residues from the C-terminus leads to reduced binding of PA to cells (34). The low degree of sequence homology shared by PA, *iota-Ib* and VIP1 in domain 4 is expected if the three proteins bind to different host cell receptors.

**b. EF/LF binding.** The removal of PA<sub>20</sub> exposes a high-affinity binding site ( $K_d = 10$  pM) for LF or EF on PA<sub>63</sub> (11). Subdomain 1*b* is a likely candidate for binding EF/LF because the removal of PA<sub>20</sub> exposes a large previously inaccessible surface on this subdomain. This agrees with the finding that antibodies recognizing an epitope between residues 168 and 314 inhibit the binding of EF/LF (33). Other antibodies

which inhibit EF/LF binding recognize an epitope between residues 581 and 601, suggesting that domain 3, which is adjacent to subdomain 1*b* (Fig. 2), may also interact with EF/LF.

**c. Heptamer formation.** Heptamer formation by the PA<sub>63</sub> fragment can be observed both in vitro and in mammalian cells (19). In electron micrographs the heptamer is ring-shaped with 7 small radial protrusions, and has an inner and outer diameter of ~20 Å and 140 Å, respectively (19).

Although the crystal structure of the heptamer has not yet been solved, we have built a hypothetical model of the heptamer which is consistent with a crystal packing analysis, electron microscopy, and sequence homology. In this model, the long axis of the monomer is oriented nearly parallel to the 7-fold symmetry axis, with domain 2 inside and domains 3 and 4 outside, such that monomers pack like pie wedges (Fig. 9).

The interface between PA<sub>63</sub> monomers involves the two faces of domain 2, which are conserved in the homologous toxins (not shown). Loop 4 of one monomer is adjacent to the cleft in domain 2 of its neighbor; it could feasibly insert into this cleft and form hydrogen bonds with an adjacent strand of the neighbor's domain 2 (see figure 5). Such a packing arrangement, involving opposite faces of a β barrel and the formation of an intermonomer β sheet, is reminiscent of the packing seen in VP1 pentamers of SV40 (35) and murine polyoma virus (36).

Our heptamer model explains why the removal of PA<sub>20</sub> (subdomain 1*a*) is a prerequisite for heptamer formation: substituting full-length PA for PA<sub>63</sub> in the heptamer model results in a severe overlap among the seven subdomains 1*a*, suggesting that this subdomain prevents oligomerization sterically.

**d. Membrane insertion.** PA<sub>63</sub> inserts into membranes at acidic pH and forms ion-conductive channels in both artificial lipid bilayers (37, 38) and cells (39). How this occurs is not immediately apparent from the PA crystal structure or the PA<sub>63</sub> heptamer model. Long hydrophobic helices have been implicated in the ability of toxins such as diphtheria toxin, colicin A, exotoxin A, and insecticidal δ-endotoxin to insert into membranes (40), but PA contains no such helices.

A possible clue comes from studies of α-hemolysin (αHL) of *Staphylococcus aureus*, a 33 kDa protein toxin which, like PA, can exist as a water-soluble monomer or as a heptameric membrane pore (41, 42). αHL contains a large loop which is exposed in the soluble monomer but is occluded in the assembled pore (43-45). In the recently determined crystal structure of the detergent-bound αHL heptamer, this loop forms an amphipathic hairpin, and the seven hairpins in the heptamer associate to form a 14-stranded, porin-like β barrel (46). The amphipathic nature of this hairpin is reflected by the pattern of alternating hydrophilic and hydrophobic residues in its sequence (Fig.

10A). A similar pattern exists in loop 2 of PA and in the corresponding residues of *iota-Ib* and VIP1 (Fig. 10A). We therefore propose that membrane insertion by PA<sub>63</sub> involves the formation of a porin-like  $\beta$  barrel, in which loop 2 plays a role analogous to that of the membrane-inserting loop of  $\alpha$ HL.

This hypothesis accounts for the following observations: (i) chymotrypsin treatment of PA (which cleaves uniquely in loop 2 without causing dissociation into two fragments) results in a loss of toxicity, but does not affect the receptor binding, LF binding, or receptor-mediated endocytosis steps of intoxication (32)(see figure 1). (ii) A deletion mutant missing the two Phe residues (F313 and F314) at the tip of loop 2 is defective in membrane channel formation and translocation of LF into the cytosol (47). (iii) The diameter of PA<sub>63</sub> membrane channels determined from ion conductance studies is  $\sim 12 \text{ \AA}$  (48), consistent with the predicted diameter of a 14-stranded  $\beta$ -barrel (49). (iv) PA<sub>63</sub> channels are highly cation selective (37), consistent with the net charge of -7 on the interior of the putative  $\beta$  barrel (Fig. 10A).

A substantial conformational change is required in domain 2 for the seven loops to form a porin-like barrel. This change could feasibly be induced during acidification of the endosome (Fig. 1, step 6). The observation that membrane channel formation is rapidly accelerated when the pH is lowered from 7.4 to 6.5 (37) implicates the titration of histidines, of which there are five (H263, H299, H304, H310 and H336) within or very close to loop 2. In crystals of PA, reducing the pH from 7.5 to 6.0 causes loop 3, which is connected to loop 2 by only 7 residues, to become disordered and expose three hydrophobic residues (Fig. 5). Although further studies are required to determine what changes occur in the PA<sub>63</sub> heptamer, one possibility is that residues connecting loop 2 to loops 1 and 3 peel away from the body of domain 2 to form an enlarged loop at the bottom of domain 2 (see figure 5). This large loop could then associate with symmetry-related loops to form the porin-like barrel (Fig.10B). These changes in domain 2 require breaking fewer hydrogen bonds than are gained upon barrel formation (and hence are thermodynamically feasible). Interestingly, a similar conformational change has recently been described to explain the pH-induced conversion of transthyretin from its native conformation to an amyloidogenic form (50).

## **CONCLUSIONS**

In the past year we have discovered several interesting features of the full-length PA molecule. Particularly significant is the finding that PA binds calcium ions, raising the possibility that calcium plays an important role in PA activity. Also of interest is the finding that a large loop in domain 2 could feasibly form an amphipathic hairpin sufficiently long to span a lipid bilayer, suggesting that the membrane-inserted form of PA may resemble that of  $\alpha$ -hemolysin.

Our work suggests a number of approaches for designing an improved anthrax vaccine. For example, the channel forming properties of PA may be responsible for some of the negative side-effects observed with the current anthrax vaccine. The deletion of loop 2 should produce a PA molecule lacking channel-forming activity but maintaining a high degree of immunogenicity. Similarly, mutations in loop 4 may result in a molecule defective in heptamer formation, and hence in channel formation. Also, it should be possible to express the individual domains (the boundaries of which have been precisely defined by our crystallographic studies) as recombinant proteins and to test these for immunogenic and protective properties. Our data also suggest a range of mutations that can be used to test the functional role of other residues on the protein surface.

Recently we have made significant progress in the structure determination of the PA<sub>63</sub> heptamer. We have determined conditions for reproducibly growing crystals in three crystal forms. From two crystal forms we have collected diffraction data at ~5 Å resolution or better. The third crystal form grows in the presence of detergent, suggesting that the heptamer may be in its membrane-inserted conformation. We intend to collect complete diffraction data sets for all three crystal forms, and will try to solve their structures by molecular replacement using search models derived from our 2.1 Å crystal structure of PA. An independent strategy is to obtain experimental phases using isomorphous heavy metal derivatives, and an encouraging first result is our success in co-crystallizing PA<sub>63</sub> in the presence of compounds known to derivatize full-length PA. The phases obtained from either the molecular replacement or the isomorphous replacement approach can be vastly improved by averaging over the 7-fold noncrystallographic symmetry, and these improved phases should greatly facilitate the task of building an accurate model of the heptamer.

Finally, the work described in this report has led to the following revised model of anthrax intoxication of the host cell: PA binds to cell receptors through domain 4, but is unable to oligomerize because of steric hindrance from subdomain 1*a*. Cleavage at the furin site followed by dissociation of PA<sub>20</sub> results in heptamer formation, chiefly mediated by domain 2. LF or EF binds to the newly exposed subdomain 1*b*, followed by receptor-mediated endocytosis of the complex. Acidification of the endocytic vesicle leads to a conformational change in the heptamer that permits seven flexible loops to insert into the membrane as a porin-like β barrel. How EF and LF are translocated across the membrane remains a puzzle, but the heptameric pore formed by PA<sub>63</sub> is clearly too small to permit the passage of EF or LF as a native folded polypeptide. A role in translocation could conceivably be played by the two calcium ions buried in the putative EF/LF binding domain: a lowered calcium concentration or a pH drop in the endosome might promote their release and modulate the PA<sub>63</sub>:EF/LF interaction.

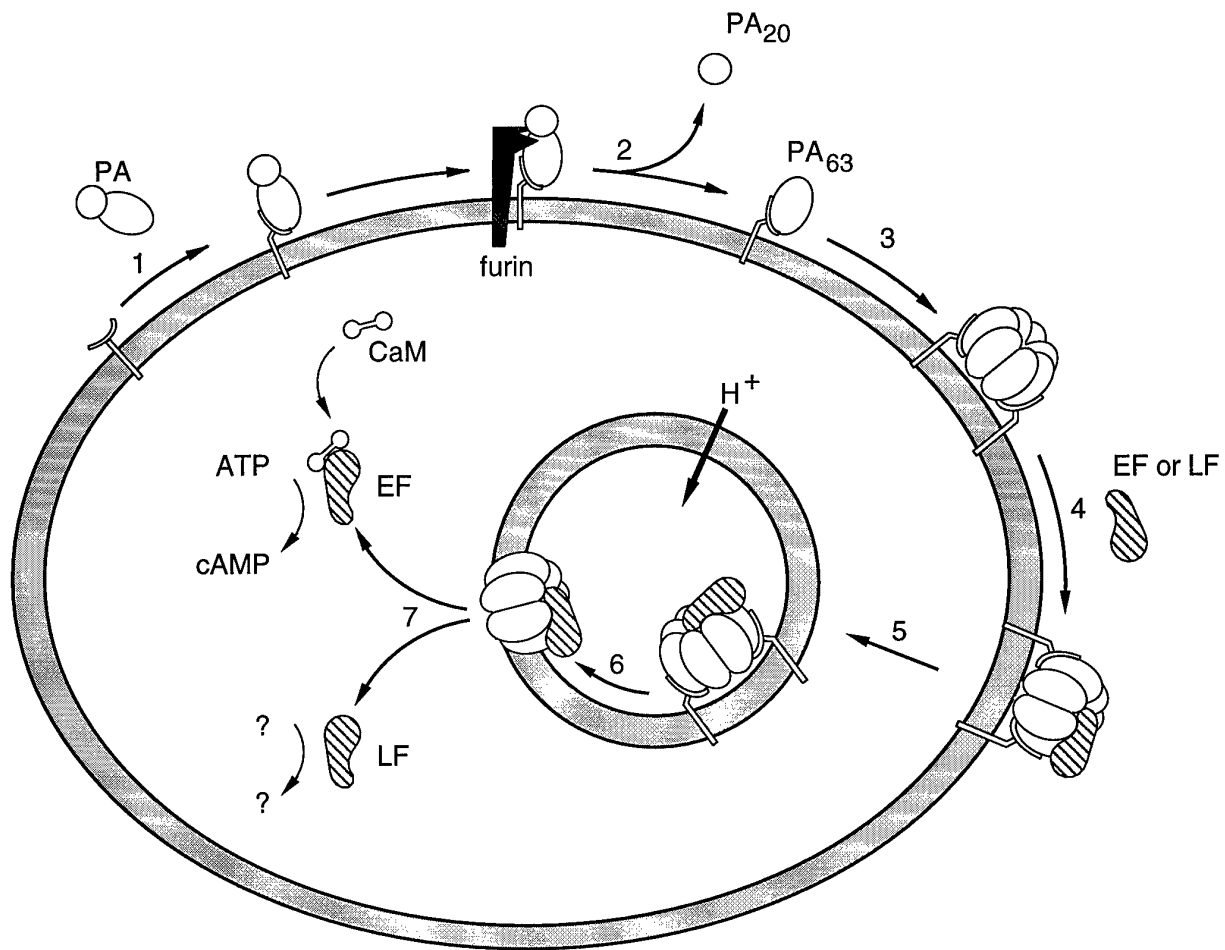


**Fig. 1.** Steps in anthrax intoxication of the host cell. The abbreviations are: PA, protective antigen; EF, edema factor; LF, lethal factor; CaM, calmodulin. 1. PA binds to a host cell surface receptor. 2. Furin or a furin-like cell surface protease cleaves PA, releasing the PA<sub>20</sub> fragment. 3. PA<sub>63</sub> forms a heptamer. 4. EF or LF binds to PA<sub>63</sub>. 5. Receptor-mediated endocytosis occurs. 6. Acidification of the endocytic vesicle leads to membrane insertion of PA<sub>63</sub>. 7. Translocation of EF/LF into the cytosol, where they exert their toxic effects.

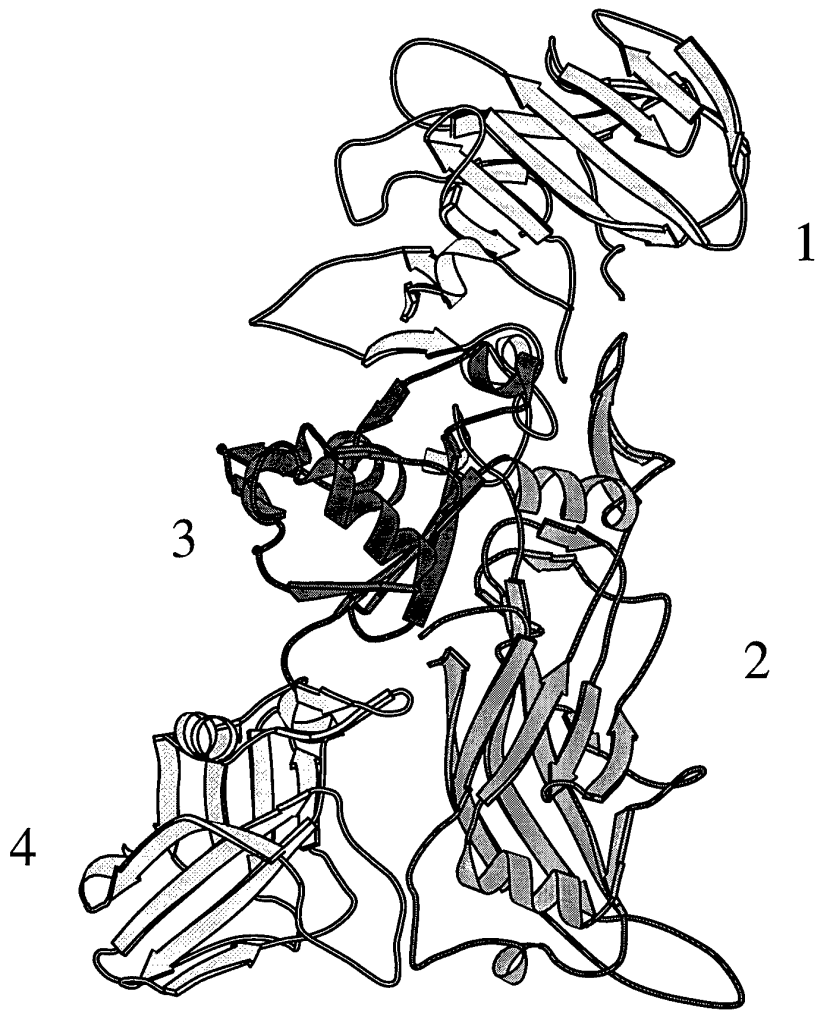
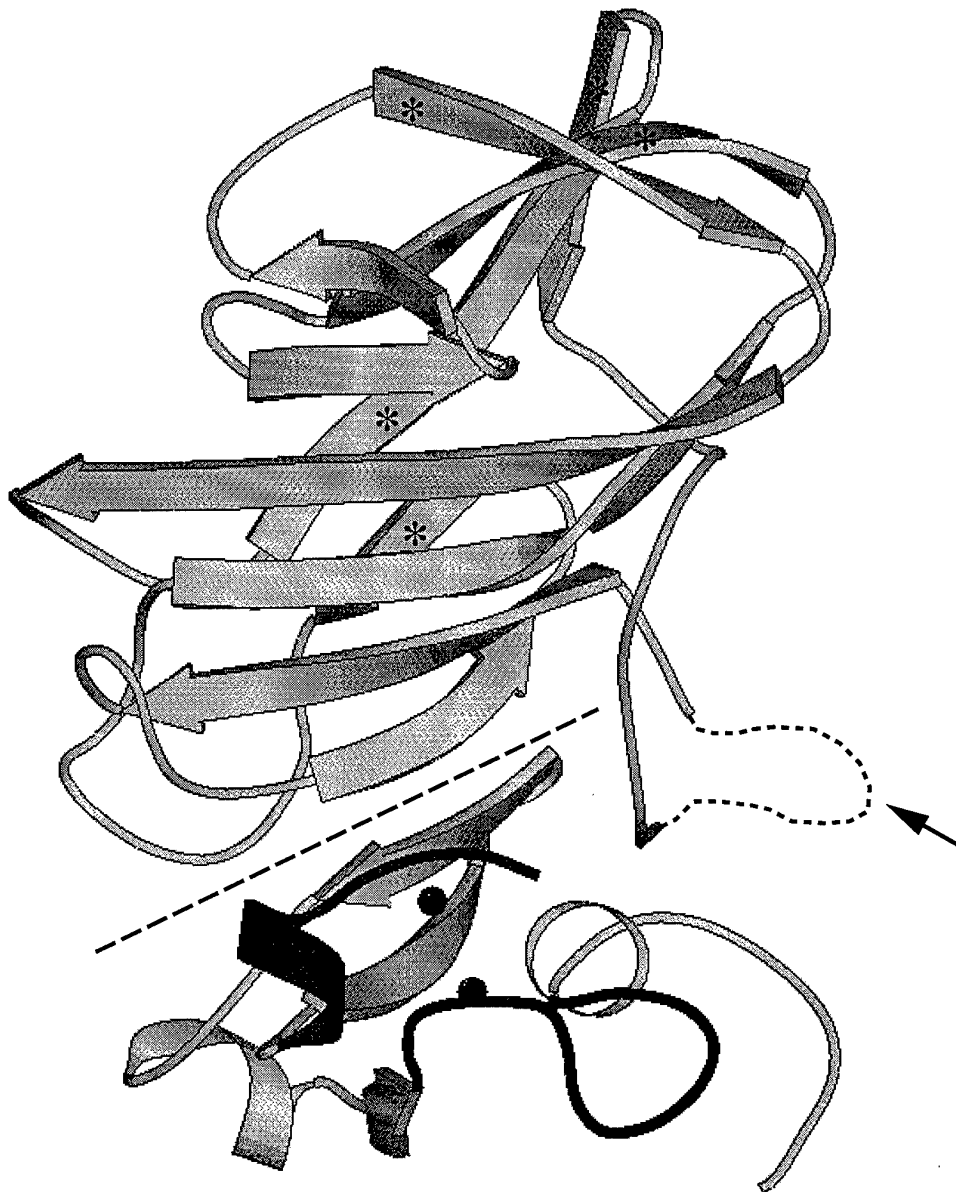
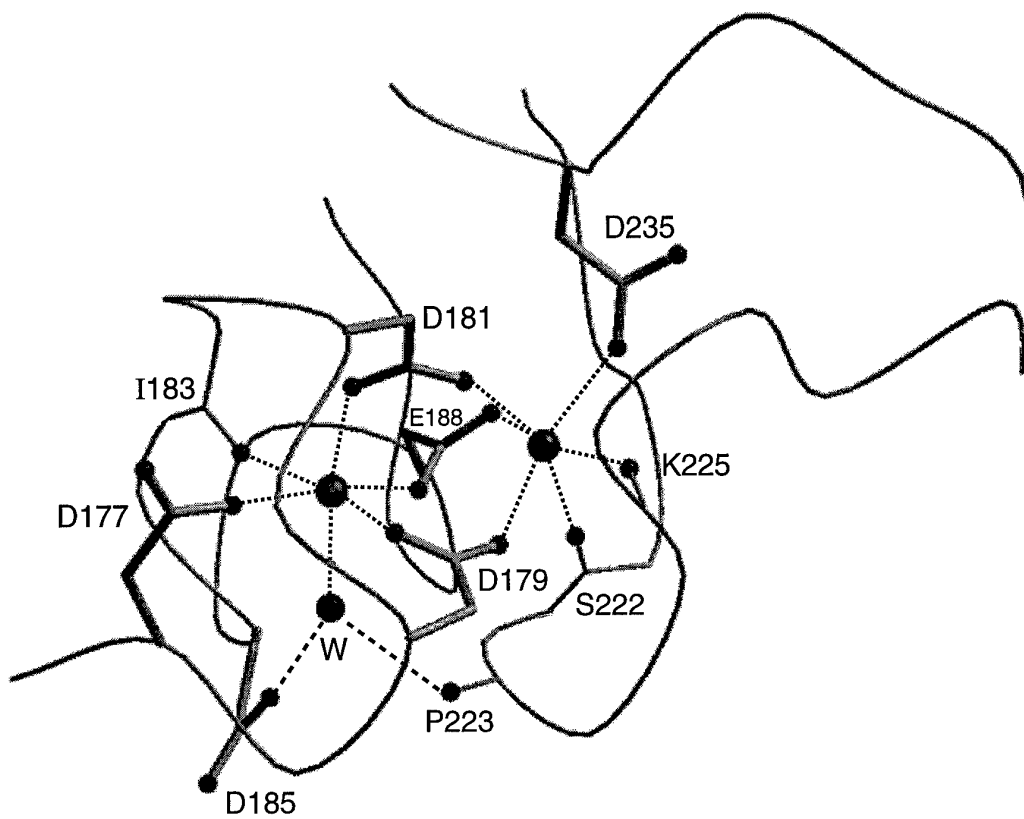


Fig.2. Ribbon diagram of PA.  
The four domains are indicated.



**Fig. 3.** Domain 1. The large  $\beta$  sheet is in the foreground and the small one, marked with asterisks, is in the background. Calcium-binding loops are highlighted and the two calcium ions are shown in black. The arrow indicates the furin cleavage site located in a disordered loop (dotted line). The dashed line separates subdomain 1*a* from 1*b*.



**Fig. 4.** The calcium binding site. The calcium ions are shown as large spheres. Ca1 (left) is coordinated by the carboxylate oxygens of D177, D179, and E188, the carbonyl oxygen of I183 and by a water molecule (W), which in turn is hydrogen bonded to a carboxylate oxygen of D185 and to the carbonyl oxygen of P223. The calcium binding loop formed by residues 177–188 conforms to the canonical EF-hand. Ca2 (right) is coordinated by carboxylate oxygens of D179, D181, E188 and D235, and the carbonyl oxygens of S222 and K225.

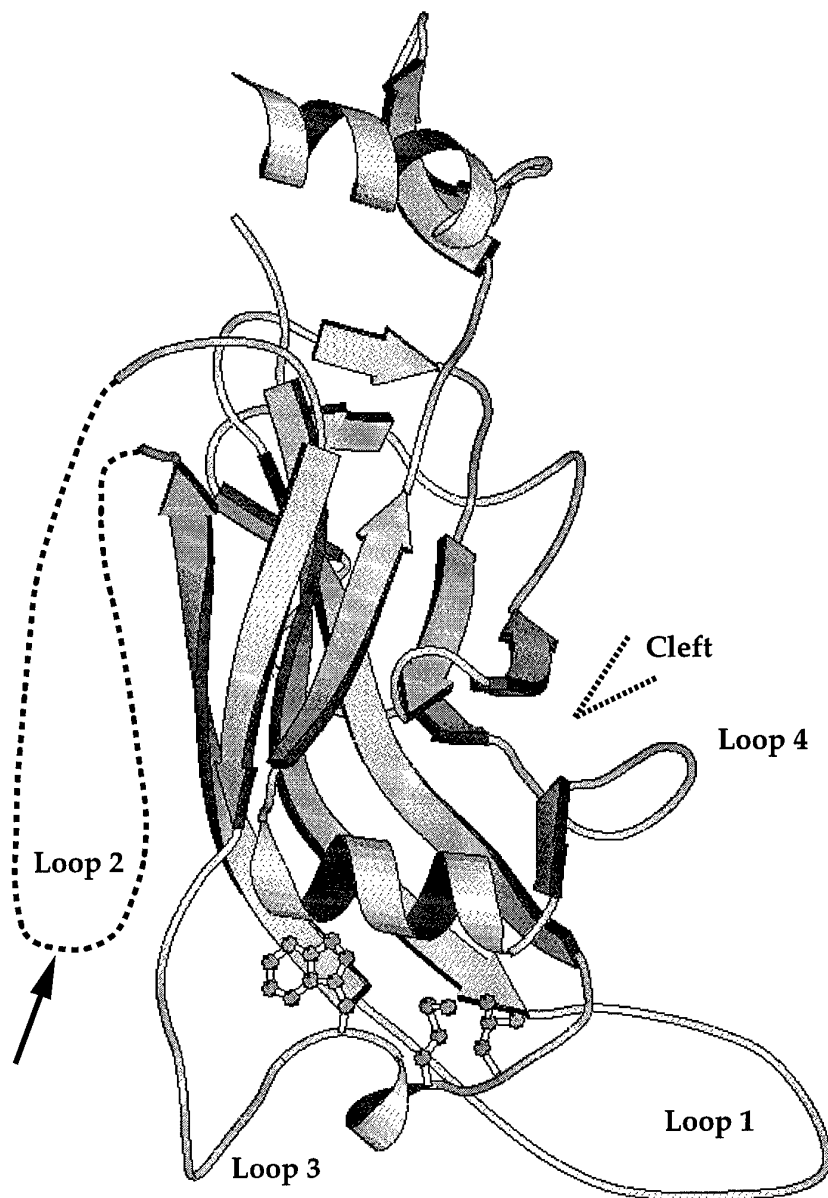


**Fig. 5.** Domain 2. Loops 1 to 4 are indicated, and the cleft in the domain is shown by the dashed wedge. The arrow indicates the chymotrypsin cleavage site in loop 2. Residues Trp346, Met350 and Leu352 of loop 3 are shown in the buried conformation they adopt in crystal form 1 (pH 7.5); they are disordered in crystal form 2 (pH 6.0).

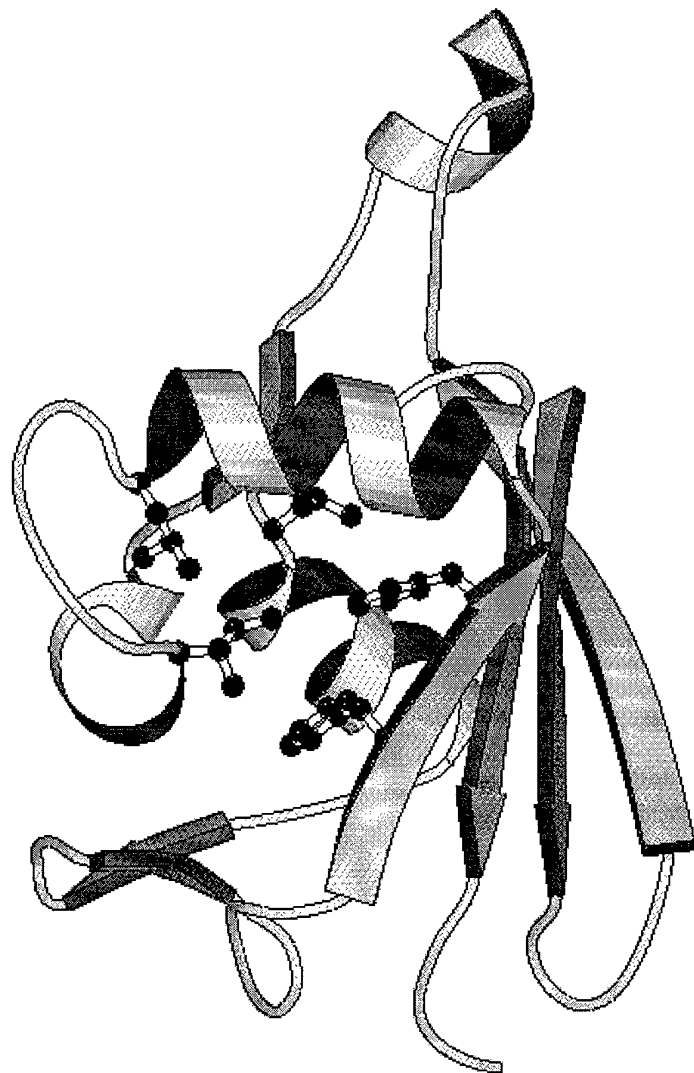


**Fig. 6.** Domain 3. The residues forming the hydrophobic patch (Phe552, Phe554, Ile562, Leu 566 and Ile574) are shown. In crystals of PA this patch is occupied by a Phe from a neighboring molecule (not shown).

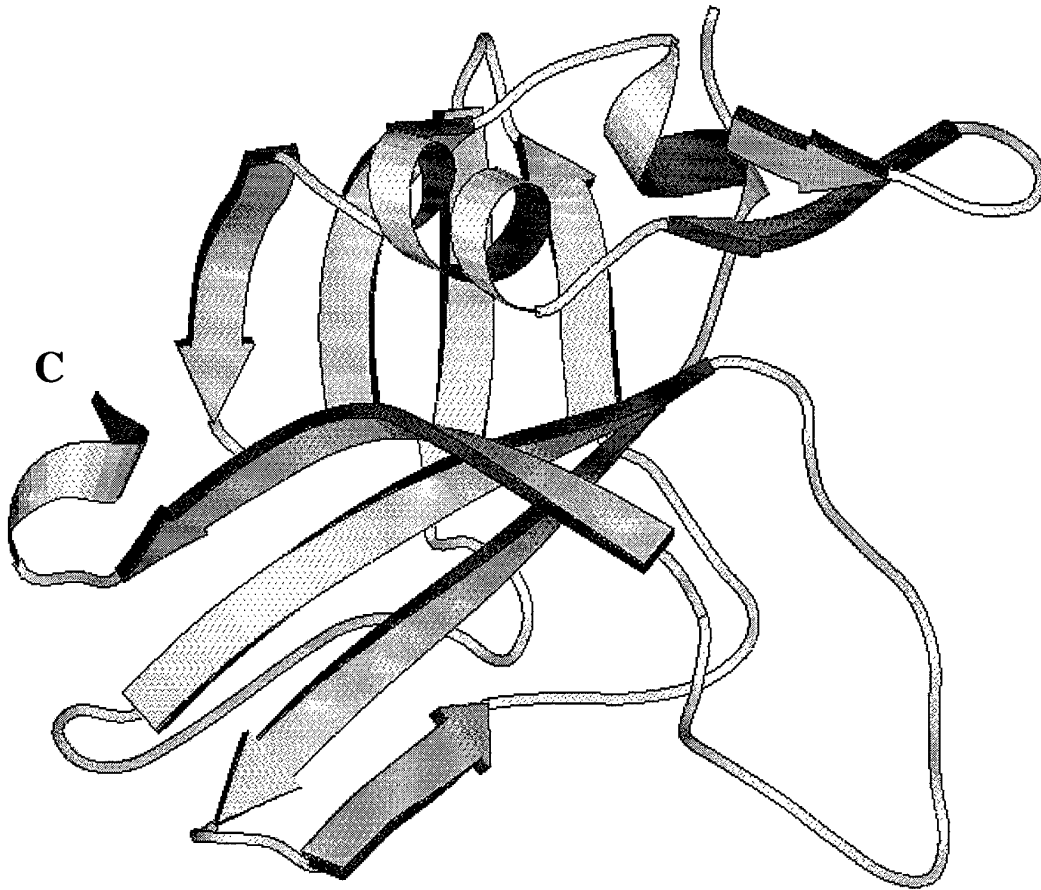


**Fig.7.** Domain 4. The C-terminus is indicated. The  $\beta$  hairpin which packs against domain 3 is at the top right and the large loop involved in the interface with domain 2 is at the bottom right.

		1β1	1β2	1β3							
PA	-----EVKQENRLNNESESSQGLLGYFFSDLNFQAPMVVTSSTTGDLSIPSSLENIIPS				55						
Ib	-----EETINENTLSSNGLMGYFFADEHFKDLELMAPIKNGDLKFEKKVVDKITE				50						
VIP1	MKNMKKLLASVVTCTLLAPMFLNGVNAVYADSKTNQISITQKNQKEMDRKGLLGYFFKGDKFSNLTMPAPTRDSTLIYDQQTANKLLD				90						
		1β4	1β5	1β6	1β7	1β8	1β9	1β10			
PA	E-NQYFQSAIWSGFEIKVKKSDEYTFATSADNHVTMWVDDQEVINKASNSNKIRLEKGRLYQIKIQYQ--RENPTKGLDFKLYWTDSD--Q								140		
Ib	D-NSSIKSIRWTGRIIPSEDEYIILSTR-NDVLMQINAKGDIKAK--TLKVNMKRQAYNRIEIQ-DKNGSIDNLSVPKLYWELN---								134		
VIP1	KKQQEYQSIRWTGRIIPSEDEYIILSTR-NDVLMQINAKGDIKAK--TLKVNMKRQAYNRIEIQ-DKNGSIDNLSVPKLYWELN---								180		
		1β11	<i>Furin</i>			1α1	1β12	1β13	1α2	1β14	
PA	NKKEVISSDNLQPELKQKS-----SNRKRKTSAGPTVPPDRDNDGIPDSLEVEGYTVDVKNKRTFLSPWISNIHEKKGLTKYK									220	
Ib	GNKTVIPEENLFRDYSKID--ENDPFIPIPNVDFVRFSSAEDLDTDNDNIPDAYEKNGYTIKDS----IAVKWNDSFAEQ--GYKKYV									214	
VIP1	NQPQQVQDELRNPEFNKESQEFELAKPSKINLFTQKREIDEDTDTGDCSTPDLWEENGYTIHNR----IAVKWDDSLASK--GYTKFV									265	
			* * * *								
		1α3	1α4	2β1	2β2						
PA	SSPEKWSIASDPYSDFEKTGRIKNSVPEARHPLVAAYPIVHVDMENILSKNEDQSTQNTDSETRTISKNTSTSRHTTSEVHGNAEVH									310	
Ib	SSYLESENTAGDPYTDYQKASGSIDKAIKLEARDPLVAAYPIVHVDMENILSKNEDQSTQNTDSETRTISKNTSTSRHTTSEVHGNAEVH									300	
VIP1	SNPLESHTVGDYTDYQKAAARDLDSNAKETFNPLVAAYPIVHVDMENILSKNEDQSTQNTDSETRTISKNTSTSRHTTSEVHGNAEVH									347	
		* * *		← loop 1 →							
<i>Chymotrypsin</i>											
		2β3	2α1	2β4	2β5	2β6	2β7				
PA	ASFFDIGGSVYAGFSNSSTVAIDHSLSLAGERIWAETMGLNADTARLNANIRYVNTGTAPIYVNLPTTSLVLGKNOTLATTAKAKENQ									400	
Ib	YNGFTGNITTSYSHTTDNGSTAVQDSNGES-----WNTGLSINKGESAYINANVRYVNTGTAPIYVNLPTTSLVLGKNOTLATTAKAKENQ									383	
VIP1	IGPKGISFGVSVNYQ--HSETVAQEWGTS--NTSQFNWASAGYLNANVRYVNTGTAPIYVNLPTTSLVLGKNOTLATTAKAKENQ									428	
		← loop 2 →	← loop 3 →								
		2β8	2β9	2β10	2β11	2α2	2β12	2β13	2β14	2α3	
PA	LSQILAPNNYYPKSNLAPIALNAODDFSSPTITMNYNQFLELEKTKQLRLDTPQVYGNIAATYVFNENGRVVDVTSNWSVLPQIQETAR									490	
Ib	IGNNLSFENETYPKKGSLPALNMDQFNARLTPINVDLKKLDSGKIKLETTQVSGNYGTKNSQ--GQIITEGNS--WSNYISQIDSVSAS									471	
VIP1	TALNISFGESYPPKKGQNGIAITSMDDFNHPIITLKKQVDNLLNKKPMMLETNQTGQVYKIKDTH--GNIVTGE--WNGVIQKAKAKTAS									515	
		← loop 4 →									
		3β1	3β2	3α1	3β3	3α2	3β4	3β5	3β6	3α3	
PA	IIFNGKDLNLVERRIAANVPSDPLETTKPDMLKEALKIAPG--FNEPNGNLQYQCKDITE--PDFNFDQOTSQNIKNQLAELNA----									571	
Ib	IIILD-TGSSQTFERRVAAKEQGNPEDKT-PELTIGEAKKAFS-ATKNGE-LLYFNGLIPE--VELIFDDNTSEIIEQKLYLDD----									550	
VIP1	IIVD-DGERVAEKRVAAKDYENPEDKT-PSLTLKDALKLSYPDEIKIEIGLLYKPKPIYESSVMTYLDENTAKEVTKQLNDTDTGKPKDV									603	
		3α4	3β7	3β8	4β1	4β2	4α1	4β3	4β4	4α2	4β5
PA	TNIYTVLDKIKLNKAKNILLIRD---KRFHYDRNNAIVGADESVVKEAH---REVINSSTEGLLNIDDKDIRKILSGYIVEIEDTEG-										651
Ib	KKIYNV---KLERGMILLIKVPSYFTNFDEYNNFPASWSNIDTKQNDG---LQSVANKLSGETKIIIPMSKLPYKRYVFSGYSKD---										630
VIP1	SHLYDV---KLTPKMNVTKLSILYDNAESNDNSIGKWTNTNIVSGGNGKQYSNNPDANLTLNTDAQEKLKNNRXYISLYMKSEK										693
		4β6	4β7	4β8	4β9						
PA	-----LKEVINDRYDMLN-----ISSLRQDGKTFIDFKKYNDKLP-----LYISNPYKVVVAVTKE									708	
Ib	-----PSTNSITVN-----IKSKEKTDYLVDTKFDLEIT-----LTSSGVIFLDNLSEILKE									684	
VIP1	NTQCEITIDGGEYPIITTKVNVNKNQNYKRLDIIAHNKSNPISLHLIKTNDDEITLFWDDISITDVASIKPENLTDSEIKQIYSRYGKLE									783	
		4β10	4α3								
PA	NTIINPSENGDTSTNGIKKI-----LIFSCKGYEIG		735								
Ib	PEIKVPSDQGNFYIDGIKEA-----L-DYIQYRVE		710								
VIP1	DGILLIDKGGIHYGEFINEASFNIEPLPNYVTKYEVTVSSELGPNVSDTLESKIIYKDGTIKFDFTKYSKNEQGLFYDSGLNWF									884	
										KINAITYDGKEMNVFHRYNK	

**Fig. 8.** Secondary structure assignment and alignment of the PA, Iota-Ib and VIP1 sequences. The numbering of each sequence is shown. Residues identical in two or more sequences are shown in bold, and those identical in all three are highlighted. The furin and chymotrypsin sites of PA are indicated, as are loops 1-4 of domain 2. Residues which ligate a calcium ion through a side chain or main chain oxygen atom are marked by an asterisk or a caret (^), respectively.



**Fig. 9.** The hypothetical model of the PA63 heptamer, viewed down the heptamer axis, with domain 1*b* nearest the viewer and domain 4 the furthest.



## REFERENCES

1. R. Koch, *Beitr. Biol. Pflanz.* **2**, 277 (1877).
2. W. S. Greenfield, *Proc. R. Soc. (London)* **30**, 557 (1880).
3. L. Pasteur, *Comptes rendus hebdomadaires des séances de l'Académie des Sciences.* **92**, 429 (1881).
4. T. Fujikura, in *Proceedings of the international workshop on anthrax* P. C. B. Turnbull, Ed. (Salisbury Medical Society, Winchester, England, 1989), vol. 68, pp. 1.
5. N. Zenova, "The deadly cloud over Sverdlovsk," *Wall Street Journal* 1990, pp. Nov. 28 p.A22.
6. P. Gumbel, "The anthrax mystery./Death in the air/The survivors speak.," *Wall Street Journal* 1991, pp. Oct. 21, p.A18; Oct 22, p.A20; Oct 23, p. A14.
7. M. Meselson, et al., *Science* **266**, 1202-8 (1994).
8. R. J. Manchec, M. G. Broster, *Nature* **294**, 254 (1981).
9. P. Turnbull, in *Topley and Wilson's Principles of Bacteriology, Virology and Immunity: Bacterial Diseases*. G. R. Smith, C. S. F. Easman, Eds. (Edward Arnold, London, 1990), vol. 3, pp. 365-79.
10. P. S. Brachman, in *Bacterial infections of humans: epidemiology and control* A. S. Evans, P. S. Brachman, Eds. (Plenum, New York, 1991) pp. 75-86.
11. S. H. Leppla, in *Sourcebook of Bacterial Protein Toxins* J. E. Alouf, J. H. Freer, Eds. (Academic Press, San Diego, 1991) pp. 277-302.
12. S. H. Leppla, in *Bacterial Toxins and Virulence Factors in Disease*. J. Moss, B. Iglewski, M. Vaughan, A. T. Tu, Eds. (Marcel Dekker, New York, 1995) pp. 543-72.
13. J. L. Stanley, J. Sargeant, H. Smith, *J. Gen. Microbiol.* **22**, 206-18 (1960).
14. A. M. Friedlander, *J. Biol. Chem.* **261**, 7123-26 (1986).
15. J. W. Ezzell, B. E. Ivins, S. H. Leppla, *Infect. Immun.* **45**, 761-7 (1984).
16. V. Escuyer, R. J. Collier, *Infect. Immun.* **59**, 3381-86 (1991).
17. K. R. Klimpel, S. S. Molloy, G. Thomas, S. H. Leppla, *Proc. Natl. Acad. Sci. U.S.A.* **89**, 10277-81 (1992).
18. V. M. Gordon, K. R. Klimpel, N. Arora, M. A. Henderson, S. H. Leppla, *Infect. Immun.* **63**, 82-87 (1995).
19. J. C. Milne, D. Furlong, P. C. Hanna, J. S. Wall, R. J. Collier, *J. Biol. Chem.* **269**, 20607-12 (1994).
20. V. M. Gordon, S. H. Leppla, E. L. Hewlett, *Infect. Immun.* **56**, 1066-69 (1988).
21. S. H. Leppla, *Proc. Natl. Acad. Sci. U.S.A.* **79**, 3162-66 (1982).
22. S. H. Leppla, *Adv. Cyclic Nucleotide Protein Phosphorylation Res.* **17**, 189-98 (1984).

23. G. M. Gill, in *Bacterial toxins and cell membranes* J. Jeljaszewicz, T. Wadstrom, Eds. (Academic Press, New York, 1978) pp. 291-314.
24. J. L. Stanley, H. Smith, *J. Gen. Microbiol.* **31**, 329-37 (1963).
25. P. Hambleton, J. A. Carman, J. Melling, *Vaccine* **2**, 125-132 (1984).
26. P. C. Turnbull, *Vaccine* **9**, 533-39 (1991).
27. B. E. Ivins, S. K. Welkos, S. F. Little, G. B. Knudson, in *Proceedings of the international workshop on anthrax*. P. C. B. Turnbull, Ed. (Salisbury Medical Society, Winchester, England, 1989), vol. 68, pp. 86-88.
28. P. C. B. Turnbull, M. G. Broster, J. A. Carman, R. J. Manchec, J. Melling, *Infect Immun* **52**, 356-63 (1986).
29. S. F. Little, G. B. Knudson, *Infect Immun* **52**, 509-12. (1986).
30. I. Pastan, V. Chaudhary, D. J. Fitzgerald, *Ann. Rev. Biochem.* **61**, 331-54 (1992).
31. S. Nakayama, R. H. Kretsinger, *Annu. Rev. Biophys. Biomol. Struct.* **23**, 473-507 (1994).
32. J. M. Novak, M.-P. Stein, S. F. Little, S. H. Leppla, A. M. Friedlander, *J. Biol. Chem.* **267**, 17186-93 (1992).
33. S. F. Little, et al., *Microbiology-UK* **142**, 707-715 (1996).
34. Y. Singh, K. R. Klimpel, C. P. Quinn, Y. K. Chaudhary, *J. Biol. Chem.* **266**, 15493-97 (1991).
35. R. C. Liddington, et al., *Nature* **354**, 278-284 (1991).
36. T. Stehle, Y. Yan, T. L. Benjamin, S. C. Harrison, *Nature* **369**, 160-3 (1994).
37. R. O. Blaustein, T. M. Koehler, R. J. Collier, A. Finkelstein, *Proc. Natl. Acad. Sci. USA* **86**, 2290-13 (1989).
38. T. M. Koehler, R. J. Collier, *Mol. Microbiol.* **5**, 1501-6 (1991).
39. J. C. Milne, R. J. Collier, *Mol. Microbiol.* **10**, 647-53 (1993).
40. M. W. Parker, F. Pattus, *Trends Biochem. Sci.* **18**, 391-395 (1993).
41. S. Bhakdi, J. Tranum-Jensen, *Microbiol. Rev.* **55**, 733-51 (1991).
42. J. E. Gouaux, et al., *Proc. Natl. Acad. Sci.* **91**, 12828-31 (1994).
43. N. Tobkes, B. A. Wallace, H. Bayley, *Biochemistry* **24**, 1915-20 (1985).
44. B. J. Walker, M. Krishnasasthy, L. Zorn, H. Bayley, *J. Biol. Chem.* **266**, 21782-86 (1992).
45. A. Valeva, et al., *EMBO J.* **15**, 1857-64 (1996).
46. J. E. Gouaux, et al., in *Am. Cryst. Assoc. Ann. Meeting* . (Montreal, 1995), vol. abstract 4m.9.A, pp. 72.
47. Y. Singh, K. R. Klimpel, N. Arora, M. Sharma, S. H. Leppla, *J. Biol. Chem.* **269**, 29039-46 (1994).
48. R. O. Blaustein, A. Finkelstein, *J. Gen. Physiol.* **96**, 905-19 (1990).

49. C. Chothia, A. G. Murzin, *Structure* **1**, 217-22 (1993).
50. J. W. Kelly, *Curr. Op. Struct. Biol.* **6**, 11-17 (1996).

## **BIBLIOGRAPHY**

*Personnel receiving pay:* Carlo Petosa, Ph.D., João Cabral, Ph.D, Christin Frederick, Ph.D, Florence Poy, Lorraine Mulry

### *Publications:*

Petosa C and Liddington RC. The anthrax toxin. In: *Protein Toxin Structure*. M. W. Parker, ed. R.G.Landes Biomedical, Austin, Texas. In press.

Petosa C, Collier RJ, Klimpel K, Leppla SH and Liddington RC. Crystal structure of the anthrax protective antigen at 2.1 Å resolution. Manuscript submitted

### *Meetings:*

C. Petosa and R.C. Liddington. Structure of the anthrax protective antigen. Annual meeting of the American Crystallographic Association, Montreal, July 1995. Vol. 23. p.61. Abstract ref. 2a.6.A.

C. Petosa and R.C. Liddington. Crystal structure of the anthrax protective antigen. Fifth international conference on Biophysics and Synchrotron Radiation, Grenoble, France, August 1995. Session 11. Abstract reference 01-25.

C. Petosa. Crystal structure of anthrax protective antigen. Gordon Research Conference on Microbial Toxins and Pathogenesis, Proctor Academy, Andover, N.H. July 1996.